10364 *Inorg. Chem.* **2009**, *48*, 10364–10370
DOI: 10.1021/ic901582j

Inorganic Chemistry
Article

$Gd_5Si_{4-x}Bi_x$ Structures: Novel Slab Sequences Achieved by Turning off the Directionality of Nearest-Slab Interactions

Volodymyr Svitlyk,[†] Branton J. Campbell,[‡] and Yurij Mozharivskyj*[,†]

[†]*Department of Chemistry, McMaster University, Hamilton, Ontario L8S 4M1, Canada, and*
[‡]*Department of Physics and Astronomy, Brigham Young University, Provo, Utah 84602*

Received August 7, 2009

Substitution of Bi for Si leads to the complete cleavage of the interslab dimers $T-T$ in the $Gd_5Si_{4-x}Bi_x$ system with $x = 1.58 - 2.42$ (T is a mixture of Si and Bi). Equivalence of the interslab $T\cdots T$ contacts, achieved through combination of the electronic and geometrical parameters, removes directionality of nearest-slab interactions and allows for a novel slab stacking. Two new slab sequences, *ABCDABCD* ($x = 2.07$, $I4_1/acd$ space group) and *ABADABAD* ($x = 2.42$, $P4_2bc$), have been discovered in $Gd_5Si_{4-x}Bi_x$ in addition to the known one, *ABAB*, that is dominant among the RE_5X_4 phases (*RE* is a rare-earth element, *X* is a *p*-element). The slab stacking for $x = 2.07$ and $x = 2.42$ is dictated by the second-nearest slab interactions which promote an origin shift either for the entire slab sequence as in *ABCDABCD* or for every other second-nearest slab pair as in *ABADABAD*. The loss of the directionality of the nearest-slab bonding allows for extensive stacking faults and leads to diffuse scattering.

Introduction

RE_5T_4 phases (where *RE* is a rare earth and *T* is a *p*-element) such as the giant magnetocaloric material $Gd_5Si_2Ge_2$ exhibit an intimate relationship between crystal structure, valence electron concentration, and physical properties.[1−9] Excluding the tetragonal Zr_5Si_4-type and hexagonal Ti_5Ga_4-type structures, most of the known RE_5T_4 structures can be described as stackings of rigid two-dimensional pseudotetragonal $_\infty^2[RE_5T_4]$ slabs (Figure 1). The principal differences among the distinct structures built from $_\infty^2[RE_5T_4]$ slabs lies in the strength of their interslab $T-T$ dimers. In Gd_5Si_4-type structures (space group *Pnma*), the slabs are interconnected by strong $T-T$ dimers ($d'_{T-T} < 2.7$ Å). In contrast, the dimers are substantially stretched (d'_{T-T} = ca. 2.9 Å) in Pu_5Rh_4 (*Pnma*) and entirely broken ($d'_{T-T} > 3.2$ Å) in Sm_5Ge_4 (*Pnma*), Eu_5As_4 (*Cmca*), and $U_2Mo_3Si_4$ ($P2_1/c$). $Gd_5Si_2Ge_2$ ($P2_1/a$) is an interesting case in which the $T-T$ dimers alternate between broken and unbroken from one interslab interface to the next.

The rigidity of these two-dimensional $_\infty^2[RE_5T_4]$ slabs and the relative flexibility of the interslab $T-T$ dimers make the overall crystal structure quite sensitive to subtle variations in the electronic and geometric parameters available via *RE* and *T*-atom substitution. Extensive research has already demonstrated that the interslab $T-T$ dimers, and thus the RE_5T_4 structures, can be manipulated by modifying either the valence electron count or the *T*-atom size.[5,9−11] In fact, the RE_5T_4 slab-stacking sequence proves to be an excellent probe of the strength of these dimers. In most cases, however, the original and modified structures are both described by the same two-slab *ABAB* stacking sequence (Figure 1), where the relative positions of the slabs are dictated by the lengths and orientations of the $T-T$ dimers. Even when the dimers are cleaved ($d'_{T-T} > 3.2$ Å), the original *ABAB* stacking sequence generally remains (e.g., the Gd_5Si_4−to−Sm_5Ge_4 transitions in the $Gd_5Si_{4-x}P_x$,[5] $Gd_5Ga_xGe_{4-x}$,[10] $Gd_5Si_{4-x}Ge_x$,[12] and $Dy_5Si_{4-x}Ge_x$[13] systems) suggesting that the residual interslab interactions are highly directional.

*To whom correspondence should be addressed. E-mail: mozhar@mcmaster.ca.

(1) Pecharsky, V. K.; Gschneidner, K. A., Jr. *Phys. Rev. Lett.* **1997**, *78*, 4494–4497.
(2) Pecharsky, V. K.; Gschneidner, K. A., Jr. *J. Alloys Compd.* **1997**, *260*, 98–106.
(3) Choe, W.; Pecharsky, V. K.; Pecharsky, A. O.; Gschneidner, K. A., Jr.; Young, V. G., Jr.; Miller, G. J. *Phys. Rev. Lett.* **2000**, *84*, 4617–4620.
(4) Choe, W.; Miller, G. J.; Meyers, J.; Chumbley, S.; Pecharsky, A. O. *Chem. Mater.* **2003**, *15*, 1413–1419.
(5) Mozharivskyj, Y.; Choe, W.; Pecharsky, A. O.; Miller, G. J. *J. Am. Chem. Soc.* **2003**, *125*, 15183–15190.
(6) Pecharsky, V. K.; Pecharsky, A. O.; Mozharivskyj, Y.; Gschneidner, K. A.; Miller, G. J. *Phys. Rev. Lett.* **2003**, *91*, 207205/01-04.
(7) Mozharivskyj, Y.; Pecharsky, A. O.; Pecharsky, V. K.; Miller, G. J. *J. Am. Chem. Soc.* **2005**, *127*, 317–324.
(8) Wu, L.-M.; Kim, S.-H.; Seo, D.-K. *J. Am. Chem. Soc.* **2005**, *127*, 15682–15683.
(9) Misra, S.; Miller, G. J. *J. Am. Chem. Soc.* **2008**, *130*, 13900–13911.
(10) Svitlyk, V.; Miller, G. J.; Mozharivskyj, Y. *J. Am. Chem. Soc.* **2009**, *131*, 2367–2374.
(11) Mozharivskyj, Y.; Tsokol, A. O.; Miller, G. J. *Z. Kristallogr.* **2006**, *221*, 493–501.
(12) Pecharsky, V. K.; Gschneidner, K. A., Jr. *J. Alloys Compd.* **1997**, *260*, 98–106.
(13) Gschneidner, K. A., Jr.; Pecharsky, V. K.; Pecharsky, A. O.; Ivtchenko, V. V.; Levin, E. M. *J. Alloys Compd.* **2000**, *303−304*, 214–222.

Published on Web 10/02/2009

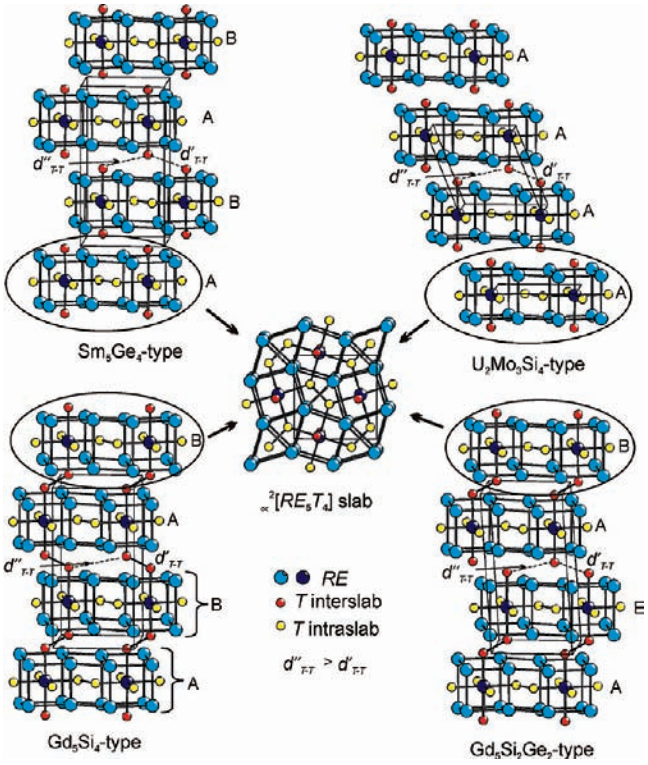

Figure 1. RE_5T_4 structure built from the $_\infty^2[RE_5T_4]$ slabs. The Eu_5As_4 structure is similar to that of the Sm_5Ge_4 but has equal $d'_{T\text{-}T}$ and $d''_{T\text{-}T}$ distances. The Pu_5Rh_4-type structure is similar to the Gd_5Si_4-type one but with the stretched $d'_{T\text{-}T}$ dimers.

In contrast to previous work, we now report that by simultaneously adjusting both valence-electron and geometric parameters within the $Gd_5Si_{4-x}Bi_x$ system, we can successfully suppress the directionality of the nearest-neighbor interslab interactions and thereby obtain entirely new slab stacking sequences that are controlled primarily by longer range (e.g., second-nearest-slab) interactions.

Experimental Section

Starting materials for $Gd_5Si_{4-x}Bi_x$ samples were pieces of gadolinium (99.99 wt.%, distilled grade, Metall Rare Earth Limited, China), silicon (99.999 wt.%, Alfa Aesar), and bismuth (99.998 wt.%, Alfa Aesar). Samples with $x = 0$, 0.5, 1, 1.5, 2.0, 2.5, 3.0, and 3.5 and a total mass of 1 g were prepared by arc-melting. During the arc-melting process, Bi pieces were placed under the Si and Gd pieces in order to minimize Bi losses associated with the high vapor pressure of molten Bi. In addition, 2 mg of extra Bi were added to compensate for anticipated losses. The samples were remelted two times to improve homogeneity. The cast samples were then sealed in evacuated silica tubes, annealed at 800 °C for 2 weeks, and quenched in cold water.

Phase analyses of the polycrystalline products were performed on a PANalytical X'Pert Pro diffractometer with a linear X'Celerator detector. Co$K\alpha$ radiation was used to avoid the Gd fluorescence associated with Cu$K\alpha$ radiation and to obtain the resolution required for the identification of structurally similar phases. Data from the samples with $x = 0$, 0.5, 1.5, 2, and 2.5 suggested phases closely related to the Gd_5Si_4-type structure. The samples with $x = 3.0$ and 3.5 yielded Gd_4Bi_3 and GdSi phases. The sample with $x = 1$ yielded a phase with a different structure and composition that is not discussed here.

Single crystals were extracted from both the cast and annealed samples with $x = 0.5$, 1.5, 2.0, and 2.5. Room-temperature data were collected on a STOE IPDS II diffractometer with Mo Kα radiation. Numerical absorption corrections were based on the crystal shapes that were originally derived from optical face indexing but later optimized against equivalent reflections using the STOE *X-Shape* software.[14] Structural refinements were performed using the *SHELXL* program.[15] Further details of the crystal structure investigations can be obtained from the Fachinformationszentrum Karlsruhe, 76344 Eggenstein-Leopoldshafen, Germany (fax: (49) 7247−808−666; e-mail: crysdata@fiz.karlsruhe.de), on quoting the depository CSD numbers 420923 for $x = 0.5$, 420922 for $x = 1.5$, 420921 for $x = 2.0$, and 420920 for $x = 2.5$, and also from the Supporting Information.

Results and Discussion

Structural Analysis. All crystals except for $x = 0.5$ showed significant diffuse scattering (Figures 2 and 3) due to stacking-fault defects in the $_\infty^2[Gd_5T_4]$ slab-stacking sequence (recall that T is the mixture of Si and Bi). This diffuse scattering was most intense at $x = 2.5$. In each case, the observed diffuse scattering obeyed an $h + k = 2n+1$ selection rule (equivalent to $k + l = 2n+1$ in the setting used for $x = 1.5$), in addition to a rather unusual $h \neq 3n$ and $k \neq 3n$ selection rule (equivalent to $k \neq 3n$ and $l \neq 3n$ in the setting selected for $x = 1.5$). The origin of these selection rules is discussed in more detail below.

Space-group determinations and structure solutions were straightforward for the crystals with $x = 0.5$, 1.5, and 2.0. Crystallographic data and atomic parameters are summarized in Tables 1 and 2 and illustrated in Figure 5. Because the diffraction data from the annealed and unannealed crystals were very similar, only the results from the annealed crystals are presented here. Indexing of the Bragg's reflections for the crystal with $x = 0.5$ yielded an orthorhombic *Pnma* symmetry and an *ABAB* slab-stacking sequence similar to that of Gd_5Si_4. The refined composition $Gd_5Si_{3.904(8)}Bi_{0.096(8)}$ of the Gd_5Si_4-type phase from the sample with $x = 0.5$ suggests that the homogeneity region for the Gd_5Si_4-type phase is unlikely to extend beyond $x = 0.096(8)$. For the crystal with $x = 1.5$, one of the indexing choices was a *C*-centered unit cell with the *b* and *c* parameters being equal within 2 standard deviations (Table 1). The orthorhombic symmetry was verified through the powder diffraction which clearly indicated peak splitting and yielded a larger difference between the *b* and *c* parameters ($a = 15.262(1)$, $b = 7.9144(8)$, $c = 7.9333(8)$ Å). The resulting structure had the *Cmca* symmetry, an *ABAB* slab-stacking sequence, and was isostructural to Eu_5As_4. But unlike Gd_5Si_4, the cleaved dimers allowed the "*B*" slab to shift all the way to the symmetric ($x = 1/2$, $y = 0$) position relative to the "*A*" slab. The crystal with $x = 2.0$ was unambiguously indexed in a larger *I*-centered tetragonal cell ($a = 7.9858(9)$, $c = 30.700(6)$ Å) and had systematic absences consistent with space-group symmetry $I4_1/acd$. The *c*-axis cell-doubling relative to the $x = 1.5$ structure is due to a novel spiral slab-stacking sequence of the *ABCDABCD* type, which involves four different symmetric in-plane slab positions: *A*(0, 0), *B*(1/2, 0), *C*(1/2, 1/2), and *D*(0, 1/2).

(14) STOE; Cie *X-SHAPE Version 2.05 and X-RED32 Version 1.10*; STOE & Cie GmbH: Darmstadt, Germany, 2004.

(15) Sheldrick, G. M. *SHELXL97 and SHELXS97*; University of Gottingen: Germany, 1997.

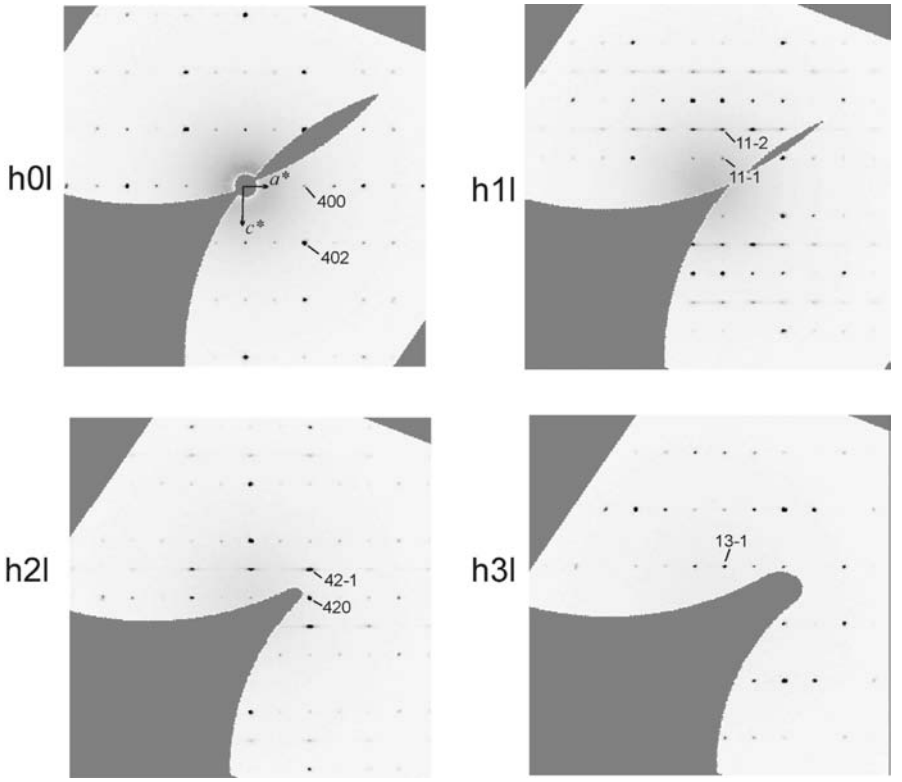

Figure 2. Reciprocal layers for the $Gd_5Si_{2.5}Bi_{1.5}$ crystal.

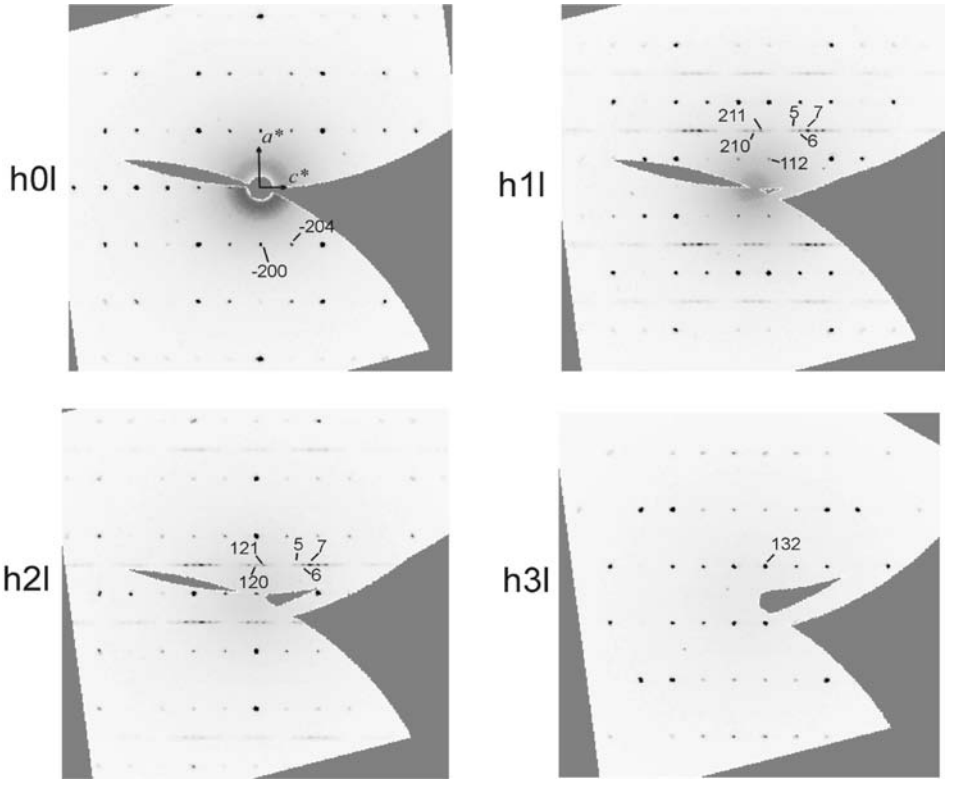

Figure 3. Reciprocal layers for the $Gd_5Si_{1.5}Bi_{2.5}$ crystal.

Stacking faults present in $Gd_5Si_{4-x}Bi_x$ structures interrupt the $_\infty^2[RE_5T_4]$ slab-stacking sequence, effectively replacing every *A* slab with a *C* slab and every *B* slab with a *D* slab (and vice versa) on one side of the fault plane. In structural refinements, this faulting is manifested as a small residual electron density within the slabs at positions that are shifted in-plane by (1/2, 1/2) relative to normal heavy atom positions. This density is most noticeable at fault-shifted Gd positions within the 3^2434 nets. In the $x = 2.5$ sample, however, which had the highest concentration of

Table 1. Crystal Data and Structure Refinements for $Gd_5Si_{4-x}Bi_x$ at 293 K, Mo$K\alpha_1$ Radiation, STOE IPDS II Diffractometer

sample	$Gd_5Si_{3.5}Bi_{0.5}$	$Gd_5Si_{2.5}Bi_{1.5}$	$Gd_5Si_2Bi_2$	$Gd_5Si_{1.5}Bi_{2.5}$
composition	$Gd_5Si_{3.904(8)}Bi_{0.096(8)}$	$Gd_5Si_{2.416(8)}Bi_{1.584(8)}$	$Gd_5Si_{1.93(1)}Bi_{2.07(1)}$	$Gd_5Si_{1.58(1)}Bi_{2.42(1)}$
space group	*Pnma*	*Cmca*	$I4_1/acd$	$P4_2bc$
lattice parameters, Å	a = 7.4850(8) b = 14.776(1) c = 7.7700(7)	a = 15.246(4) b = 7.901(2) c = 7.898(2)	a = 7.9858(9) c = 30.700(6)	a = 8.0296(7) c = 30.883(4)
volume, Å^3	859.3(1)	951.3(4)	1957.8(5)	1991.2(4)
Z	4	4	8	8
density (calc), g/cm^3	7.082	8.276	8.649	8.860
θ range	2.96 to 29.19°	2.67 to 29.15°	2.65 to 29.16°	1.32 to 25.12°
index ranges	$-10 \le h \le 10$, $-20 \le k \le 17$, $-9 \le l \le 10$	$-20 \le h \le 19$, $-10 \le k \le 9$, $-10 \le l \le 10$	$-9 \le h \le 10$, $-10 \le k \le 10$, $-41 \le l \le 42$	$-9 \le h \le 9$, $-9 \le k \le 8$, $-36 \le l \le 36$
reflections collected	7954	3268	7461	9675
independent reflections	1195 [R_{int} = 0.1191]	660 [R_{int} = 0.1424]	646 [R_{int} = 0.1289]	1778 [R_{int} = 0.1776]
completeness to max 2θ	98.9%	99.0%	96.6%	99.5%
data/restraints/par.	1195/0/48	660/0/28	647/0/26	1778/1/88
goodness-of-fit on F^2	0.952	0.855	0.997	0.735
final R indices [$I > 2\sigma(I)$]	R_1 = 0.0474, wR_2 = 0.0557	R_1 = 0.0456, wR_2 = 0.0437	R_1 = 0.0452, wR_2 = 0.0394	R_1 = 0.0531, wR_2 = 0.1224
R indices (all data)	R_1 = 0.0928, wR_2 = 0.0626	R_1 = 0.1338, wR_2 = 0.0553	R_1 = 0.1361, wR_2 = 0.0508	R_1 = 0.1936, wR_2 = 0.1666
absolute structure factor	n/a	n/a	n/a	0.0(2)
extinction coefficient	0.00046(7)	0.000059(15)	0.000037(6)	0.000048(12)
largest peak/ hole, e/Å^3	2.217/−3.448	2.289/−2.579	2.564/−1.948	2.622/−2.878
minority fraction	0	0.059(2)	0.025(2)	0.084(2)

stacking faults, the more weakly scattering Si-rich T site inside the trigonal prism also produced some fault-shifted residual electron density. The extra fault-shifted electron density was treated as a split site during the refinement, such that the occupancies of all fault-shifted atoms were constrained to be the same. The resulting occupancy is referred to as the "minority fraction" in Table 1 and is explained in the detailed description of the refinement contained in the Supporting Information. The atomic parameters of the unshifted structure are shown in Table 2, while the constraints that tie the fault-shifted and unshifted atoms together are also described in the Supporting Information.

The x = 2.5 Structure. The x = 2.5 case was comparatively complicated and will be discussed separately below. While the conventional cell shape (a = 8.0296(7), c = 30.883(4) Å) of the x = 2.5 crystal was essentially the same as that of the x = 2.0 crystal, there were many moderately weak reflections that violated the I-centering selection rule ($h + k + l = 2n$), but which were consistent with a primitive lattice (Figure 3). Oddly, these weaker I-center-violating reflections only appear within the diffuse streaks with $h + k = 2n + 1$ lines and never at the $h + k = 2n$ positions. Such a pattern is not consistent with any standard set of systematic absences. Careful examination revealed that all of the peaks along the $h + k = 2n + 1$ lines (whether or not they violate the I centering) are somewhat diffuse along the $\mathbf{c}^*$ direction and that their diffuse tails actually give rise to the observed diffuse streaks.

By neglecting the "primitive" reflections along the $h + k = 2n + 1$ lines, the structure was solved in space group $I4_1/acd$, which produced a structure similar to that of x = 2.0, except that significant residual density was found around the Gd and Si/Bi sites. While the $I4_1/acd$ solution demonstrated that the structure is built from the $_\infty^2[Gd_5T_4]$ slabs, the presence of additional "primitive" reflections suggested a different slab-stacking sequence. Various stab-stacking models based on $_\infty^2[Gd_5T_4]$ slabs were constructed, and their diffraction patterns were simulated using the ISODISPLACE software[16] and compared against the experimental diffraction data from the x = 2.5 crystal. The *ABADABAD* slab stacking, which has the $P4_2bc$ symmetry, yielded an excellent match between the simulated and experimental patterns (Figure 4) and was subsequently subjected to a successful structural refinement.

Structure of and Interactions between the $_\infty^2[RE_5T_4]$ Slabs. At this point, we will briefly discuss the structure of the $_\infty^2[RE_5T_4]$ slabs and the interslab $T-T$ interactions directing their stacking. The Gd_5Si_4, Pu_5Rh_4, Sm_5Ge_4 (*Pnma*), Gd_5Si_2Ge ($P2_1/a$), and $U_2Mo_3Si_4$−type ($P2_1/c$) structures of RE_5T_4 (see Figure 1) are built from nearly identical pseudotetragonal 3^2434 nets of RE atoms (light blue). Two such nets are stacked over one another to form $_\infty^2[RE_5T_4]$ slabs with RE atoms (dark blue) located in pseudocubes and half of the T atoms (yellow) in trigonal prismatic voids. Since the trigonal prisms in these slabs share a face, the separation between the T atoms is small enough to allow the formation of the intraslab dimers. The RE pseudocubes are capped top and bottom by exterior T atoms (red), which we refer to as the interslab T atoms. In all RE_5T_4 structures, the symmetry of the $_\infty^2[RE_5T_4]$ slabs is either tetragonal or pseudotetragonal.

As mentioned in the Introduction, the difference between different RE_5T_4 structures lies in how the $_\infty^2[RE_5T_4]$ slabs are interconnected through the interslab $T-T$ dimers. If the dimers are short ($d'_{T\text{-}T}$ < 2.7 Å), Gd_5Si_4-type structures form. If the dimers are stretched ($d'_{T\text{-}T}$ = ca. 2.9 Å) or broken ($d'_{T\text{-}T}$ > 3.2 Å), Pu_5Rh_4, Sm_5Ge_4, or $U_2Mo_3Si_4$−type structures result. And if only half of the dimers are broken, $Gd_5Si_2Ge_2$-type structures appear (Figure 1). Changes in the dimer length are accompanied by movement of the $_\infty^2[RE_5T_4]$ slab primarily along the direction of the dimer stretching/cleavage. Regardless of whether or not the dimers are broken, the T···T interslab contacts are not uniform along the dimer direction, i.e.

(16) Campbell, B. J.; Stokes, H. T.; Tanner, D. E.; Hatch, D. M. *J. Appl. Crystallogr.* **2006**, *39*, 607–614.

Table 2. Atomic and Isotropic Temperature (U) Parameters for $Gd_5Si_{4-x}Bi_x$ from Single Crystal Diffraction Data

atom	site	occupancy	x/a	y/b	z/c	U (Å^2)
			$Gd_5Si_{3.904(8)}Bi_{0.096(8)}$			
Gd(1)	8*d*	1	0.02582(9)	0.59735(4)	0.1826(1)	0.0121(2)
Gd(2)	8*d*	1	0.3190(1)	0.12269(4)	0.1793(1)	0.0105(2)
Gd(3)	4*c*	1	0.1479(1)	1/4	0.5110(1)	0.0100(2)
Si/Bi(1)	8*d*	0.952/0.048(4)	0.1551(6)	0.0389(2)	0.4698(4)	0.019(1)
Si(2)	4*c*	1	0.0249(8)	1/4	0.1007(7)	0.011(1)
Si(3)	4*c*	1	0.2656(8)	1/4	0.8717(7)	0.007(1)
			$Gd_5Si_{2.416(8)}Bi_{1.584(8)}$			
Gd(1)	16*g*	1	0.12840(6)	0.8295(1)	0.83011(9)	0.0177(2)
Gd(2)	4*b*	1	1/2	0	0	0.0120(4)
Bi/Si(1)	8*d*	0.792/0.206(4)	0.29187(8)	0	0	0.0125(4)
Si(2)	8*f*	1	0	0.8779(11)	0.1255(7)	0.014(2)
			$Gd_5Si_{1.93(1)}Bi_{2.07(1)}$			
Gd(1)	32*g*	1	0.3331(2)	0.9178(2)	0.06149(2)	0.0163(2)
Gd(2)	8*a*	1	0	1/4	3/8	0.0116(2)
Bi/Si(1)	16*d*	0.938/0.062(6)	0	1/4	0.97841(2)	0.0135(3)
Si/Bi(2)	16*f*	0.902/0.098(5)	0.3658(3)	x+1/4	1/8	0.011(1)
			$Gd_5Si_{1.58(1)}Bi_{2.42(1)}$[a]			
Gd(1A)	8*c*	1	0.6754(8)	0.1615(8)	0.06388(8)	0.043(2)
Gd(2A)	8*c*	1	0.6692(8)	0.1583(7)	0.93612(8)	0.046(2)
Gd(3A)	4*a*	1	0	0	0.9987(3)	0.034(2)
Gd(1B)	8*c*	1	0.1693(7)	0.1699(7)	0.3137(1)	0.026(1)
Gd(2B)	8*c*	1	0.1604(7)	0.1652(6)	0.1864(1)	0.026(1)
Gd(3B)	4*a*	1	0	1/2	0.2478(3)	0.024(1)
Bi(1)	4*a*	1	0	0	0.1033(2)	0.033(2)
Bi(2)	4*a*	1	0	0	0.8965(2)	0.035(2)
Bi(3)	4*b*	1	0	1/2	0.3511(2)	0.039(2)
Bi(4)	4*b*	1	0	1/2	0.1459(2)	0.024(1)
Si/Bi(5A)	8*c*	0.789/0.211(5)	0.6409(17)	0.8666(17)	0.9974(6)	0.037(3)
Si/Bi(5B)	8*c*	0.789/0.211(5)	0.1422(12)	0.8647(11)	0.2470(5)	0.025(2)

[a] For $Gd_5Si_{1.58(1)}Bi_{2.42(1)}$, the A and B labels in the atomic names designate the *A* and *B* slabs to which the atoms belong.

there are ***two*** distinct sets of $T\cdots T$ distances ($d'_{T\text{-}T}$ and $d''_{T\text{-}T}$ in Figure 1). For example, $Gd_5Si_{2.75}P_{1.25}$ which has the largest reported $T\cdots T$ distances, still has short and long interslab TT contacts ($d'_{T\text{-}T}$ = 3.74 Å vs $d''_{T\text{-}T}$ = 4.38 Å).[10] Depending on the arrangement of the $T\cdots T$ contacts between the slabs, two slab-stacking sequences can be formed: the *ABAB* sequence with its herringbone pattern of shorter $T\cdots T$ contacts and the *AAAA* sequence with its ascending pattern of shorter $T\cdots T$ contacts (Figure 1). In both cases, it is the presence of shorter and longer $T\cdots T$ contacts that provides directionality to the slab stacking. The question can be asked, "What will happen to the slab-stacking sequence in general if the interslab $T\cdots T$ contacts become uniform?". The $Gd_5Si_{4-x}Bi_x$ system provides some answers to this question.

Interslab Dimer Cleavage. There are three structural transitions in the $Gd_5Si_{4-x}Bi_x$ system as a function of the Bi concentration (Figure 5): the *Pnma* → *Cmca* transition for x = 0.10−1.58, *Cmca* → $I4_1/acd$ for x = 1.58−2.07, and $I4_1/acd$ → $P4_2bm$ for x = 2.07−2.42 (x is the refined Bi amount). The *Pnma* → *Cmca* transition in the $Gd_5Si_{4-x}Bi_x$ system (x = 0.10−1.58) features complete cleavage of the interslab T-T dimers ($d'_{T\text{-}T}$ = 2.63 → 4.15 Å) so that the $T\cdots T$ contacts all become identical. This dimer cleavage is the consequence of electronic and size effects associated with Bi substitution and mirrors the transitions observed in $Gd_5Si_{4-x}P_x$ and $Gd_5Si_{4-x}Sn_x$.[10,11] In $Gd_5Si_{4-x}P_x$, an increase in the valence electron count achieved through P substitution was used to break the interslab dimers in $Gd_5Si_{2.75}P_{1.25}$ ($d'_{T\text{-}T}$ = 2.49 → 3.74 Å).[10] In the $Gd_5Si_{4-x}Sn_x$ system, the larger size of the Sn atoms was employed to stretch the dimers ($d'_{T\text{-}T}$ = 2.49 → 3.04 Å).[11] Similar to $Gd_5Si_{2.75}P_{1.25}$, the electronic contribution to the dimer cleavage in $Gd_5Si_{2.42}Bi_{1.58}$ is related to the population of the antibonding states within the $T-T$ dimers. Also, the larger size of Bi atoms promotes dimer cleavage. The two effects can be already seen in $Gd_5Si_{3.90}Bi_{0.10}$ which shows considerable dimer stretching compared to Gd_5Si_4 ($d'_{T\text{-}T}$ = 2.49 → 2.63 Å).

In $Gd_5Si_{2.42}Bi_{1.58}$, both the electronic and size effects act in parallel and lead to the full cleavage of the interslab dimers. The resulting uniformity of the $T\cdots T$ contacts creates an additional translational symmetry element of $1/2\boldsymbol{a} + 1/2\boldsymbol{b}$, which leads to the *Cmca* space group symmetry. The full dimer cleavage also allows the slabs to relax into a pseudotetragonal state that is very near to their ideal tetragonal state, so the that b and c cell parameters become highly similar. In fact, it is only the influence of the nontetragonal stacking arrangement that prevents the slabs from becoming perfectly tetragonal. Because the ideal $_\infty^2[Gd_5T_4]$ slab has tetragonal point symmetry, it seems natural that slab-stacking sequences that are compatible with tetragonal symmetry should exist. Yet in $Gd_5Si_{2.42}Bi_{1.58}$, we continue to see a preference for the *ABAB* stacking sequence associated with unbroken dimers.

Stacking Rules and Interslab Correlations. A further increase in the Bi concentration finally yields two new and fully tetragonal slab-stacking sequences (and symmetries): *ABCDABCD* ($I4_1/acd$) for $Gd_5Si_{1.93}Bi_{2.07}$ and *ABADABAD* ($P4_2bm$) for $Gd_5Si_{1.58}Bi_{2.42}$. Consider the four in-plane slab origins permitted by uniform $T\cdots T$ contact distances: $A(0,0)$, $B(1/2,0)$, $C(1/2,1/2)$, and $D(0,1/2)$. If we label all of the slabs in the crystal with sequential integers, assuming that the zeroth slab is of the *A* type, any stacking sequence built from these four slab origins will have the following properties: (1) even-integer slabs will either be of the *A* or *C* type and (2) odd-integer slabs will either be of the *B* or *D* type. Thus, *AC*, *CA*, *BD*, and *DB* nearest-neighbor (1*NN*) pairs are never permitted.

Both the *ABCDABCD* and *ABADABAD* sequences involve four-slab stacking sequences, hence a $c \sim 30$ Å cell parameter. Unlike the *ABAB* sequence of $Gd_5Si_{2.42}Bi_{1.58}$, neither four-slab stacking sequence possesses an absolute preference for the direction of nearest-neighbor slab correlations − the neighbor of an *A* slab is equally likely to be of the *B* or *D* varieties, and the neighbor of a *B* slab is equally likely to be of the *A* or *C* varieties. Yet both sequences show a perfect correlation among fourth-nearest-neighbor slabs (4*NN* slabs) which must be of the same type. The difference rests in the nature of their second-nearest-neighbor (2*NN*) interslab correlations.

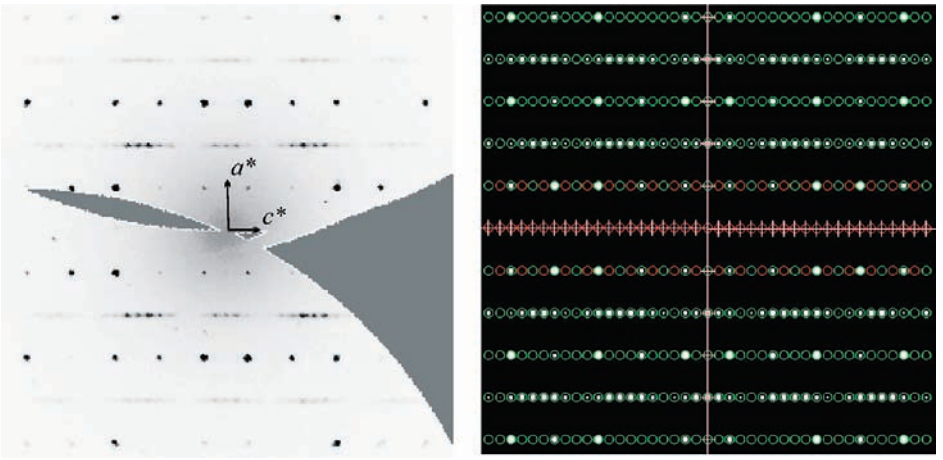

Figure 4. Comparison between the experimental (left) and simulated reciprocal (right) *h*1*l* layers for the $Gd_5Si_{1.5}Bi_{2.5}$ crystal. The *ABAD* slab sequence ($P4_2bc$ space group) was used for the simulation. In the simulated pattern, red circles mark systematically absent reflections, while green circles mark all other reciprocal lattice reflections.

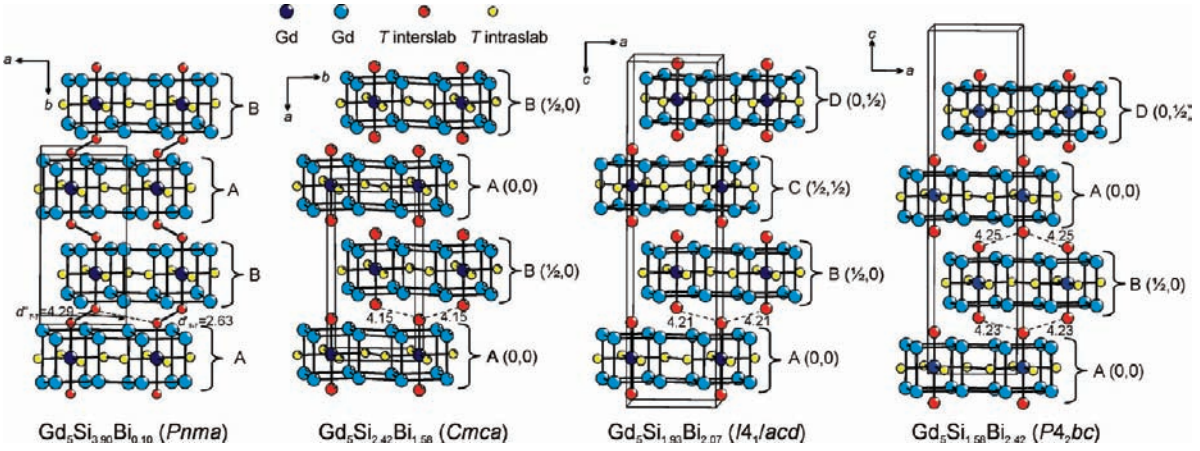

Figure 5. Structures of and slab stacking in the $Gd_5Si_{4-x}Bi_x$ phases.

For *ABCDABCD*, all 2*NN* pairs are perfectly anticorrelated (i.e., *A* pairs with *C* and *B* pairs with *D*). In contrast, for *ABADABAD*, half the 2*NN* pairs are correlated (i.e., two slabs of the same type) and half are anticorrelated.

Systematic Absences. The primary $h + k = 2n+1$ selection rule for the diffuse streaks arises from a fault vector of (1/2, 1/2, 0), which corresponds to randomly replacing an *A*(0,0) slab with a *C*(1/2, 1/2) slab or a *B*(1/2, 0) slab with a *D*(0, 1/2) slab. The stacking disorder effectively steals intensity from the Bragg peaks along these lines and redistributes it into their diffuse tails along the c^* direction.

From Figures 2 and 3, we observe that the density of Bragg reflections along the $h + k = 2n + 1$ lines is four times higher than the corresponding density along the $h + k = 2n$ lines for the $x = 2.5$ crystal. A similar observation applies to the $x = 2.0$ crystal, where the Bragg peak density is two times higher along the $h + k = 2n+1$ lines than along the $h + k = 2n$ lines. This is a strong evidence for the rigidity of the $_\infty{}^2[Gd_5T_4]$ slabs. If the slabs were to substantially relax via all of the structural degrees of freedom provided by $P4_2bc$ (or $I4_1/acd$) symmetry, then additional peaks would also appear along the $h + k = 2n$ lines consistent with the symmetry. But rigidity rather than symmetry prevents them from doing so. Thus, the unusual pattern of absences within the $h + k = 2n$ lines is due to the fact that all four slabs remain approximately identical even though they are permitted by symmetry to differ.

The unusual $h \neq 3n$ and $k \neq 3n$ diffuse-scattering selection rule observed in all of the $Gd_5Si_{4-x}Bi_x$ samples is more subtle but also less interesting. It originates in the X-ray structure factor of a single $_\infty{}^2[Gd_5T_4]$ slab, which can be factored out to the front of the overall diffuse-scattering structure factor. Or more specifically, it originates in the positions of the Gd atoms within the slab. As an example, consider a single tetragonal $_\infty{}^2[RE_5T_4]$ slab, where the average *a*-axis separation between Gd atoms within the 3^2434 nets is approximately $\Delta x_{Gd} = 1/6$. It turns out that if we set $\Delta x_{Gd} = 1/6$ exactly, and neglect all non-Gd atoms, we compute $|F_{slab}|^2 = 0$ for any $h + k = 2n + 1$ position in which $h = 3n$ or $k = 3n$, and $|F_{slab}|^2 \approx (6N_{Gd})^2$ for each of the other $h + k = 2n + 1$ positions, where N_{Gd} is the atomic number of Gd. In Figure 6, which illustrates the distribution of $|F_{slab}|^2$ intensities for a single slab of $Gd_5Si_{1.93}Bi_{2.07}$, we see that the selection rule is only approximate since there are other atoms contributing to the structure factor.

In Figure 3, observe that the intensity of the diffuse streaks from the $x = 2.5$ crystal and also the intensities of the Bragg peaks along the same $h + k = 2n + 1$ lines are

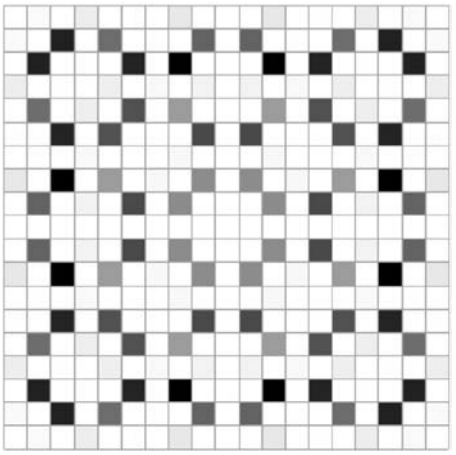

Figure 6. Distribution of $|F_{slab}|^2$ intensities for the $h+k = 2n+1$ positions within the $l = 0$ plane of $Gd_5Si_{1.93}Bi_{2.07}$ for $-9 \le h, k \le 9$. The square at the center corresponds to $h = 0$ and $k = 0$. Darker squares indicate higher intensities. The $h+k = 2n$ squares are left empty − their intensities are not represented here.

modulated along the c^* direction with a period roughly equal to 4 r.l.u. (relative to a short cell parameter corresponding to a two-slab stacking sequence). More generally, the diffuse scattering in all of the $Gd_5Si_{4-x}Bi_x$ samples was modulated along c^* (a^* for $x = 1.5$) with roughly the same period. This rather striking feature also has its origin in $|F_{slab}|^2$, which contains a multiplicative factor of $\cos^2(2\pi/\Delta z_{Gd})$, where Δz_{Gd} is the c-axis separation between the Gd2 atoms inside the tetragonal voids and the Gd1 atoms within the 3^2434 nets. Measured in r.l.u. relative to a two-slab cell parameter, this separation is approximately $\Delta z_{Gd} = 0.127$, which yields a period of $\Delta l = (2z_{Gd1})^{-1} = 3.94 \approx 4$ r.l.u., as observed.

Conclusions

The $Gd_5Si_{4-x}Bi_x$ system highlights the role of next-nearest-slab interactions in the structural assembly in the RE_5T_4 phases. Interslab $T-T$ dimers or residual bonding left from these dimers (i.e., the $T\cdots T$ contacts are not equivalent) serves as a directional force for the $_\infty{}^2[RE_5T_4]$ slab packing and leads to the *ABAB* and *AAAA* stacking sequences. The complete cleavage of the $T-T$ dimers in $Gd_5Si_{4-x}Bi_x$ switches off this directionality and produces novel slab sequences. In cases when $T\cdots T$ interactions provide no directionality, the second-nearest-slab interactions become important. In particular when these interactions are strong and promote an origin shift, a four-slab *ABCDABCD* sequence results. If the second-nearest-neighbor interactions favor the same origin, the *ABAB* order persists, and the presence of the two types of interactions promotes the formation of *ABADABAD* stacking. Strong second-nearest-slab interactions promote long-range stacking order, while weaker interactions or competing interactions lead to stacking disorder and diffuse scattering. Currently, the physical nature of the second-nearest-slab interactions that produced the observed interslab correlations in $Gd_5Si_{4-x}Bi_x$ is being investigated.

Acknowledgment. This work was supported by a Discovery Grant from the Natural Sciences and Engineering Research Council of Canada and by an award from Research Corporation.

Supporting Information Available: Discussion of the relationship between the residual electron and fault densities, refinement procedures and results for $Gd_5Si_{4-x}Bi_x$ with $x = 1.58$, 2.07, and 2.42, and X-ray crystallographic files for $x = 1.58$, 2.07, and 2.42 (CIF). This material is available free of charge via the Internet at http://pubs.acs.org.